Chemical Science

ROYAL SOCIETY OF CHEMISTRY

EDGE ARTICLE

View Article Online
View Journal | View Issue

Cite this: *Chem. Sci.*, 2024, **15**, 4860

All publication charges for this article have been paid for by the Royal Society of Chemistry

Received 22nd August 2023
Accepted 24th January 2024

DOI: 10.1039/d3sc04412b

rsc.li/chemical-science

Kinetically controlled synthesis of rotaxane geometric isomers†

Dillon R. McCarthy,‡[a] Ke Xu, ‡[b] Mica E. Schenkelberg,[ab] Nils A. N. Balegamire,[ab] Huiming Liang,[a] Shea A. Bellino,[a] Jianing Li [ab] and Severin T. Schneebeli *[ab]

Geometric isomerism in mechanically interlocked systems—which arises when the axle of a mechanically interlocked molecule is oriented, and the macrocyclic component is facially dissymmetric—can provide enhanced functionality for directional transport and polymerization catalysis. We now introduce a kinetically controlled strategy to control geometric isomerism in [2]rotaxanes. Our synthesis provides the major geometric isomer with high selectivity, broadening synthetic access to such interlocked structures. Starting from a readily accessible [2]rotaxane with a symmetrical axle, one of the two stoppers is activated selectively for stopper exchange by the substituents on the ring component. High selectivities are achieved in these reactions, based on coupling the selective formation reactions leading to the major products with inversely selective depletion reactions for the minor products. Specifically, in our reaction system, the desired (major) product forms faster in the first step, while the undesired (minor) product subsequently reacts away faster in the second step. Quantitative ^{1}H NMR data, fit to a detailed kinetic model, demonstrates that this effect (which is conceptually closely related to minor enantiomer recycling and related processes) can significantly improve the intrinsic selectivity of the reactions. Our results serve as proof of principle for how multiple selective reaction steps can work together to enhance the stereoselectivity of synthetic processes forming complex mechanically interlocked molecules.

Complex interlocked molecules have become integral components for the development of next-generation supramolecular catalysts,[1] molecular machines,[2] and molecular motors.[3] In particular, rotaxanes with either oriented tracks[4] or facially dissymmetric macrocycles[5] have shown promise for ribosome-inspired peptide synthesis[6] and cargo transport.[7] To impart additional degrees of spatial control and unidirectionality into these systems, it would be desirable to combine oriented axles with facially dissymmetric (*i.e.* rim-differentiated) macrocyclic components in a selective fashion, which leads to geometric isomers.[8]

We now report a through-space controlled[9] aminolysis reaction, which can selectively form specific geometric isomers of [2]rotaxanes under kinetic control. Our approach starts with a readily accessible [2]rotaxane with a symmetric axle, which is then desymmetrized based on selective stopper exchange accelerated[10] by the presence of nearby glyme functional groups. We have recently applied this concept in the context of interlocked molecules with through-space glyme-activating groups (Fig. 1a), which enabled the two reactive ends in rotaxanes to communicate with each other.[10] However, in our initial system, the ring components of the rotaxanes were facially symmetrical. Therefore, our initial system did not address the complexity of forming specific rotaxane geometric isomers selectively, which has now been accomplished in this work. Furthermore, in our initial glyme-catalyzed rotaxane system (Fig. 1a), we had observed only modest selectivity for the glyme-activated reactions with the maximum selectivity for mono- *vs.* difunctionalization ~8 : 1 at the beginning of the reaction.[10] Overall, our glyme-activated directional stopper-exchange process represents an alternative way to accomplish kinetic selection of reaction barriers in interlocked molecules. Our results complement existing approaches to control/augment chemical reactivity through space across the mechanical bond.[11] Related processes have also been implemented in chemically fueled molecular machines, where the position[2a,12] or facial dissymmetry[13] of the macrocycle determine the rate of addition and/or removal or a barrier.

Here, we now find that the selectivity for forming specific rotaxane geometric isomers increases exponentially during such glyme-activated reactions. After ~300 hours, the d.r. for formation of the major geometric isomer increases to >40 : 1,

[a]*Departments of Chemistry, Pathology, and Materials Science Program, University of Vermont, Burlington, VT 05405, USA. E-mail: Schneebeli@purdue.edu*

[b]*Departments of Industrial & Molecular Pharmaceutics, Chemistry, and Medicinal Chemistry & Molecular Pharmacology, Purdue University, West Lafayette, IN 47907, USA*

† Electronic supplementary information (ESI) available. See DOI: https://doi.org/10.1039/d3sc04412b

‡ Equal authorship contribution.

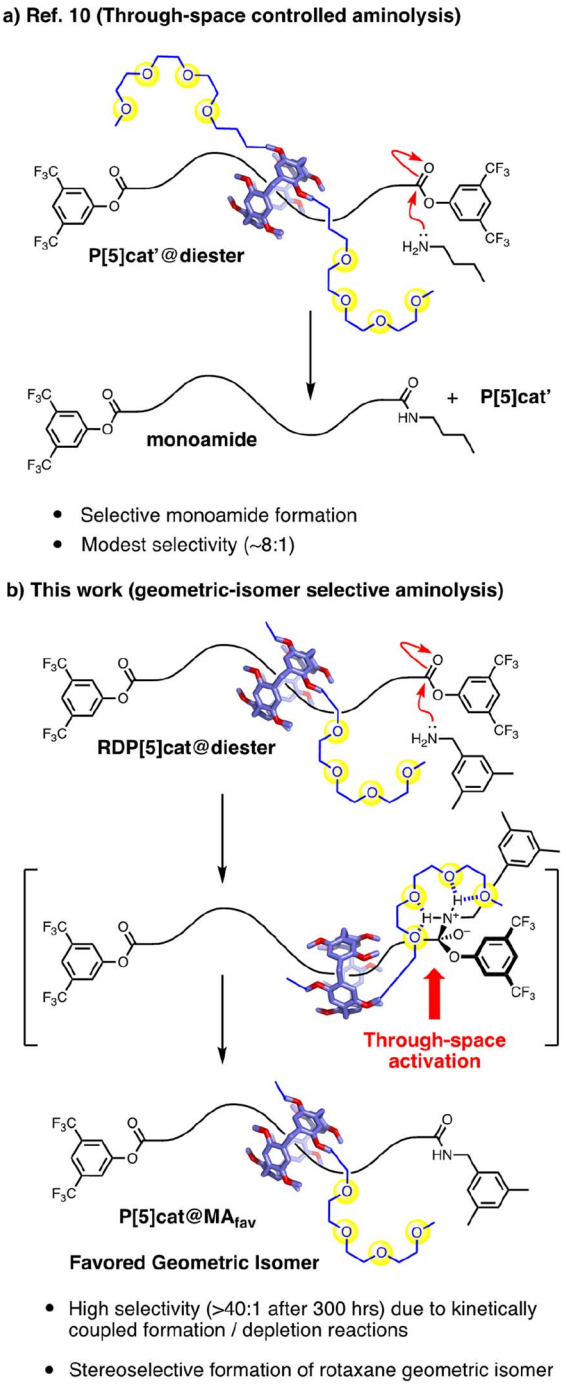

Fig. 1 (a) Through-space controlled aminolysis in a rotaxane system. (b) This work applies the concept to the selective synthesis of rotaxane geometric isomers, while also introducing a strategy to enhance the selectivity in such reactions by coupling (see also Scheme 1) a formation reaction selective for the major geometric isomer with a depletion reaction with inverse selectivity.

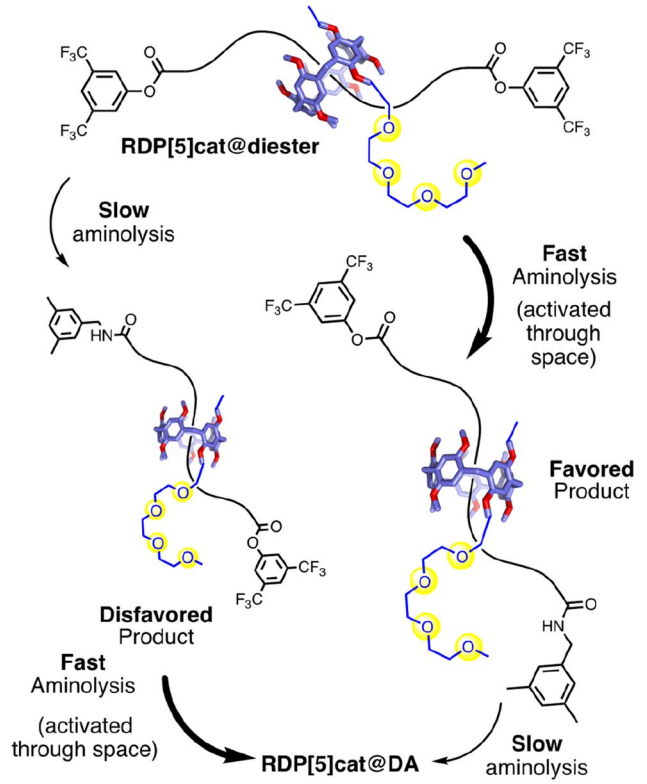

Scheme 1 A matrix of fast and slow aminolysis reactions (all fast ones are through-space controlled by the glyme-activating groups) leads to kinetic control of geometric isomerism with >40 : 1 selectivity for the major geometric isomer.

which represents a remarkable improvement from the prior 8 : 1 ratio. Our reactions lead (Fig. 1b) to specific rotaxane geometric isomers with high selectivity. This improved selectivity was enabled by coupling (Scheme 1) two through-space controlled aminolysis reactions[8f,10,14] with each other: the first reaction leads to the major geometric isomer with modest selectivity, while the second through-space controlled aminolysis reaction selectively depletes the minor product. Thereby, the overall selectivity of the coupled reaction system is enhanced significantly compared to the two individual reactions. While this concept is related to minor enantiomer recycling[15] and related photo-deracemization processes,[16] the minor isomer is not recycled in our system. Therefore, while the selectivity rapidly increases over time (which can lead to simpler purification), the increased selectivity arises at the cost of the overall yield in our system, which decreases over time.

To establish proof-of-concept for our kinetically controlled synthesis, a rim-differentiated pillar[5]arene[17] was chosen as the facially dissymmetric macrocycle given the ease of synthesis,[18] excellent chemical stability and solubility,[19] and the ability to control the directionality of the catalyst/activating group.[17,20] The triglyme activating group (needed to selectively enhance the rate of stopper exchange as illustrated in Fig. 1b) is readily installed and is a known[10,14a–d,21] organocatalyst for aminolysis reactions in relatively nonpolar organic solvents like chloroform. With these building blocks in hand, we synthesized **RDP[5]cat@diester** (Scheme 1) in 54% yield by threading[10,22] the rim-differentiated pillar[5]arene **RDP[5]cat** (synthesis detailed in the ESI†) onto a hexadecanedioic acid dichloride axle in the presence of excess 3,5-bis(trifluoromethyl)phenol stopper and triethylamine. Next, we subjected **RDP[5]cat@diester** to aminolysis

with 3,5-dimethylbenzylamine at 30 °C. We worked up the reaction early (after 60 hours), to ensure that we could isolate both the major and the minor geometric isomers of the mono-amide products as the NMR standards for the quantitative ^{1}H NMR experiments (Fig. 3). As measured by ^{1}H NMR spectroscopy (see Fig. 3c), the minor geometric isomer disappears almost completely at later time points.

The glyme-activated stopper-exchange reaction with a first amine nucleophile (3,5-dimethylbenzylamine) led to a mixture of three aminolysis products, which included the two geometric isomers of the mono-substituted rotaxanes **RDP[5]cat@MA$_{fav}$** and **RDP[5]cat@MA$_{disfav}$**, as well as the disubstituted rotaxane **RDP[5]cat@DA** in 96% combined yield (calculated based on recovered starting material). The excess amine in the reaction mixture posed a challenge during the workup as attempts to remove the solvent increased the amine concentration, which led to the complete substitution of the remaining active esters. Therefore, we developed a protocol (see ESI† for details) to remove the excess 3,5-dimethylbenzylamine reagent by simple filtration through an acid-chloride functionalized MP carboxylic acid resin before concentration and purification of the reaction mixture.

The structures of the reaction products with the 3,5-dimethylbenzylamine nucleophile (**RDP[5]cat@MA$_{fav}$**, **RDP[5]cat@MA$_{disfav}$**, **RDP[5]cat@DA**) were confirmed with ^{1}H NMR, ^{13}C NMR, and ^{1}H–^{1}H ROESY NMR spectroscopy, as well as with high-resolution mass spectrometry (see the ESI†). Notably, the ^{1}H–^{1}H ROESY NMR spectrum of the major, monosubstituted rotaxane product **RDP[5]cat@MA$_{fav}$** (Fig. 2a) shows a cross peak between the H_{et} proton resonance (the –CH_3 proton resonance of the ethyl group on the pillar[5]arene macrocycle, observed as a triplet at 1.41 ppm) and the H_o aromatic resonance at 7.64 ppm (which corresponds to the *ortho*-protons on the remaining active-ester stoppering unit). The presence of this cross-peak seems to indicate that the pillar[5]arene macrocycle possesses an energetically favorable co-conformation, in which the ring binds to the remaining active ester stopper.

To investigate the origin of this attractive interaction between the ring and the active ester stopper, we optimized a DFT model (Fig. 2b) of the corresponding complex and calculated the noncovalent interactions from the DFT-optimized electron density with the NCI method.[23,24] Based on our DFT results, there are attractive [C–H···O] and [C–H···F] interactions (illustrated as blue spheres in Fig. 2b), which seem to be playing a key role in stabilizing the co-conformation with the pillar[5]arene macrocycle residing next to the active-ester stopper.

Finally, to confirm our kinetic model for the reaction with the 3,5-dimethylbenzylamine nucleophile, we conducted detailed kinetic studies with quantitative ^{1}H NMR spectroscopy to investigate the selectivity of the reaction over time. For this purpose, **RDP[5]cat@diester** was reacted with an excess of 3,5-dimethylbenzylamine in $CDCl_3$ at 30 °C in an NMR tube. Our reaction system is governed by four rate constants, k_1, k_1', k_2, and k_2' as defined in Fig. 3a. Reaction progression was monitored by ^{1}H NMR in $CDCl_3$ using 1,2,4,5-tetrabromobenzene (TBB) as the internal standard. The unique amide protons for all three rotaxane products were readily apparent (Fig. 3b), which allowed us to integrate them against the internal TBB standard to yield absolute concentrations. The resulting concentration–time plots (Fig. 3c) were fit to the kinetic model shown in Fig. 3a

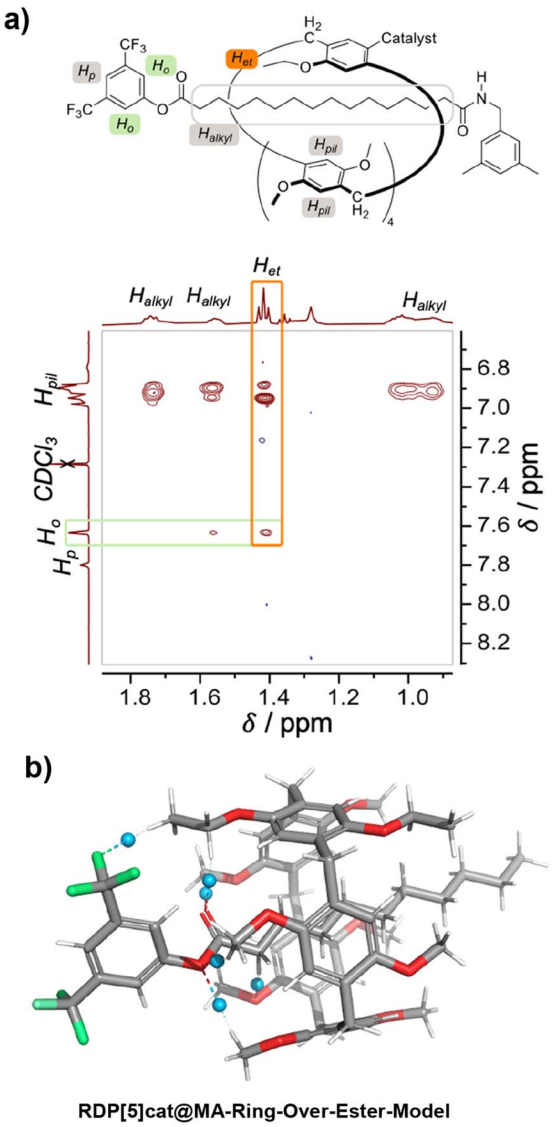

Fig. 2 (a) Partial ^{1}H–^{1}H ROESY NMR (500 MHz, $DCDl_3$) spectrum of the major geometric isomer (**RDP[5]cat@MA$_{fav}$**) obtained from the aminolysis reaction of **RDP[5]cat@diester** with 3,5-dimethylbenzylamine. See the ESI† for additional characterization data as well as the full ^{1}H–^{1}H ROESY NMR spectrum. The ^{1}H–^{1}H ROESY NMR spectrum shown in the figure clearly shows that the ethyl group on the pillar[5]arene ring is located proximal to the remaining active ester present in the axle of the favored geometric rotaxane isomer. The key NOE cross-peak between H_{et} and H_o—which leads us to this conclusion—is highlighted in orange. (b) Non-covalent interaction plots[23] calculated at the B3LYP-MM/LACVP* level of theory with the NCI method implemented in Jaguar (version 8.8) as detailed in the ESI.† The NCI plots show the presence of attractive [C–H]···F interactions between the ethyl groups on the pillararene ring and one of the –CF_3 functionalities of the 3,5-bis(trifluoromethyl)phenyl stopper. We hypothesize that these non-covalent interactions are primarily responsible for biasing the equilibrium distribution of the pillararene ring toward the side of the active-ester stopper, which results in the clear NOE cross-peak shown in panel (a).

with Dynafit,[25] providing the four rate constants k_1, k_2, k_1', and k_2'. The kinetic model showed that the rate constant corresponding to the formation of the favored rotaxane **RDP[5]cat@MA$_{fav}$-1** ($k_1 = 0.55 \pm 0.03$) is about an order of magnitude larger than the corresponding rate constant for formation of the disfavored rotaxane **RDP[5]cat@MA$_{disfav}$-1** ($k_2 = 0.08 \pm 0.005$). Moreover, both k_1 and k_1' are also about an order of magnitude larger than either k_2 or k_2', demonstrating the increased reactivity at the end of the rotaxane nearest to the catalyst.

Our Dynafit model, which was fit to the quantitative ^{1}H NMR data shown in Fig. 3c, provides concentrations of 0.70 mM for **RDP[5]cat@MA$_{fav}$-1** and 0.02 mM for **RDP[5]cat@MA$_{disfav}$-1** at ~250 hours, which leads to a selectivity of approximately 31 : 1 d.r. at this reaction time point. After 300 hours, the selectivity for the formation of the major geometric isomer rises even further to about ~45 : 1. This finding provides proof of principle for the enhanced selectivity enabled by our kinetically coupled reaction system.

With the kinetic model established for 3,5-dimethylbenzylamine as the nucleophile, we generalized (Fig. 4) our selective rotaxane synthesis to other amine nucleophiles, including 1-naphthalenemethanamine and 9-anthracenemethanamine.

Both systems performed qualitatively similar to the reaction system with the 3,5-dimethylbenzylamine, which confirms the generality of our kinetically controlled rotaxane geometric isomer synthesis. However, we also observed (Fig. 4 and 6) clear trends in the rate constants, based on (i) the sterics of the nucleophiles/amide stoppers and (ii) the sterics of the secondary (non-activating) face of the ring, which (when positioned over an active ester) seems to slow down the aminolysis reactions.

(i) Steric effects of the nucleophile/amide stopper on the aminolysis rates: First, the observed trend in k_1 rate constants (Fig. 4) clearly shows that the k_1 rate constants decrease with increasing steric bulk of the nucleophile, as one would expect for a classical acyl substitution mechanism.

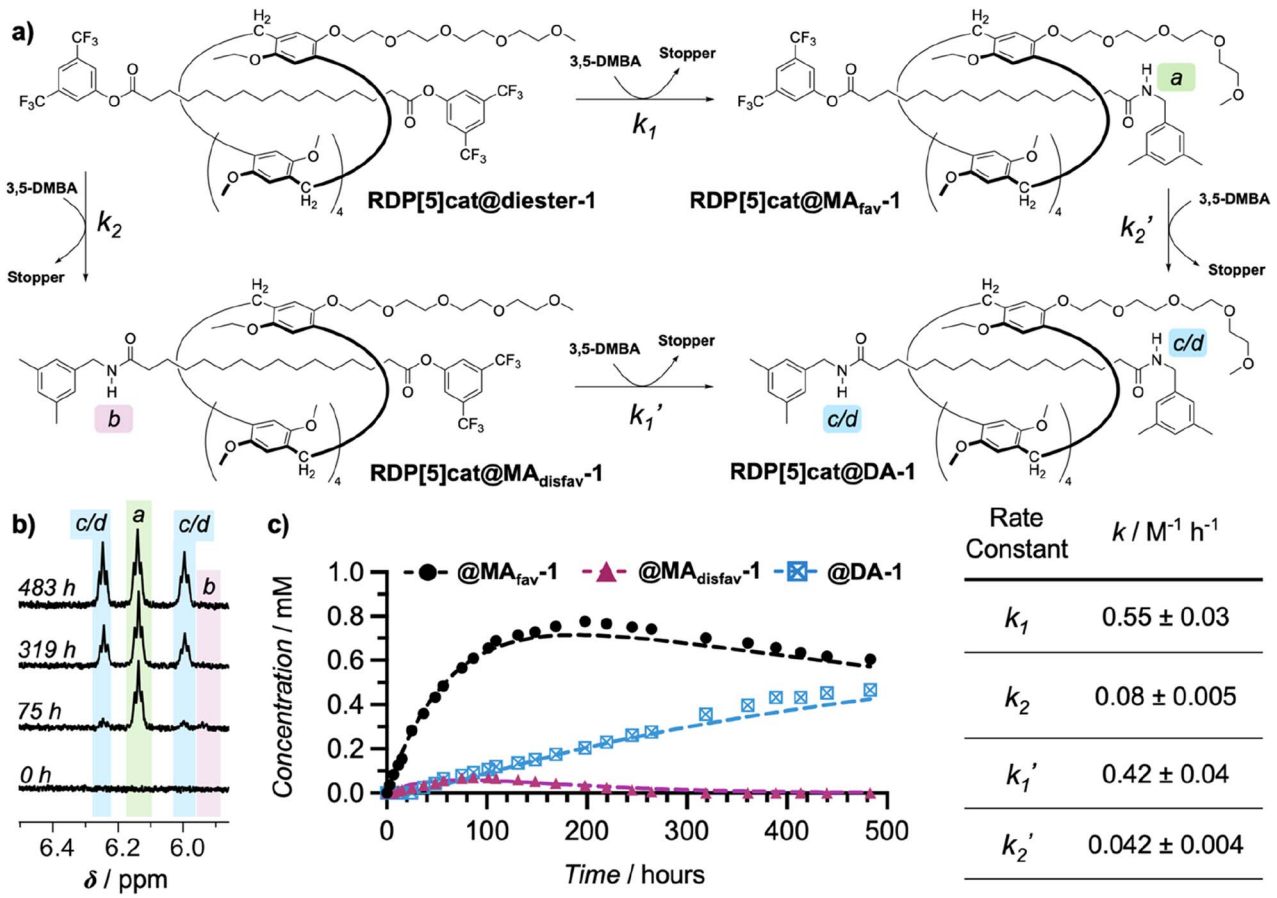

Rate Constant	k / M^{-1} h^{-1}
k_1	0.55 ± 0.03
k_2	0.08 ± 0.005
k_1'	0.42 ± 0.04
k_2'	0.042 ± 0.004

Fig. 3 (a) Complete kinetic pathway for through-space controlled stopper exchange with 3,5-dimethylbenzylamine as the nucleophile. 3,5-DMBA = 3,5-dimethylbenzylamine; Stopper = 3,5-bis(trifluoromethyl)phenol. Rate constants k_1 and k_1' denote substitution at the activated ester (proximal to the catalytic the side-chain), while k_2 and k_2' denote substitution at the ester distal to the catalyst. (b) Four representative ^{1}H NMR spectra (500 MHz, $CDCl_3$, 300 K) recorded at different time points over the course of the kinetics experiment. The three sets of amide protons (1 NH each for both **RDP[5]cat@MA$_{fav}$** and **RDP[5]cat@MA$_{disfav}$**, 2 NH for **RDP[5]cat@DA**) are highlighted. A complete stack of the entire kinetics spectrum is shown in Fig. S1 in the ESI.† (c) Concentrations of all three reaction products measured by quantitative ^{1}H NMR spectroscopy with the TBB internal standard over the course of the reaction. The reaction was run at 30 °C as detailed in the ESI.† Kinetics fits are shown as dashed lines. The kinetic fits were obtained using the Dynafit software package as detailed in the ESI.† Derived rate constants with error bars (standard errors obtained from the Dynafit kinetic fits) are shown in the table on the right.

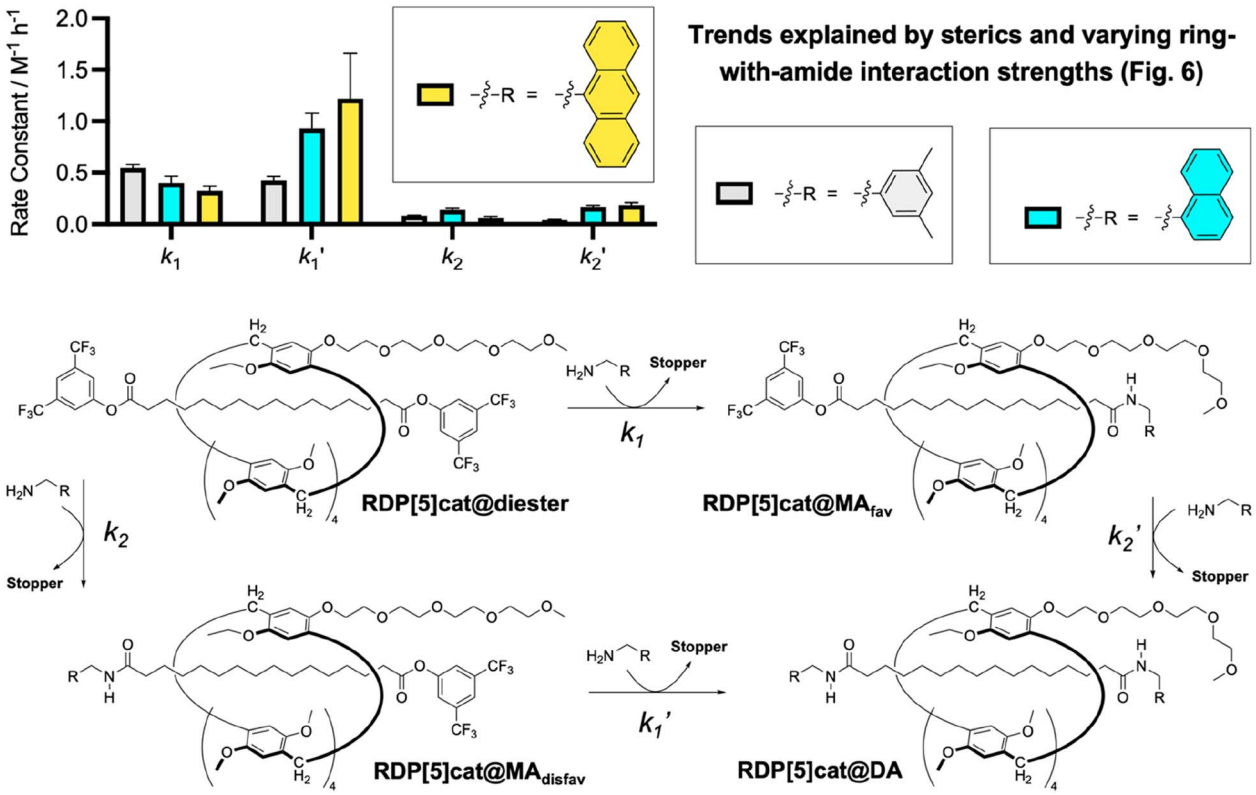

Fig. 4 Comparison of aminolysis rate constants for RDP[5]cat@diester with different amine nucleophiles. All reactions were run at 30 °C as detailed in the ESI.† See Fig. S1–S5† for the kinetic fits and stacks of the time-dependent ^{1}H NMR spectra, which were used to determine all the rate constants. The kinetic fits were obtained using the Dynafit software package as detailed in the ESI.† Numerical values for the derived rate constants with error bars (standard errors obtained from the Dynafit kinetic fits) are listed in Fig. 3c, S3b, and S5b.†

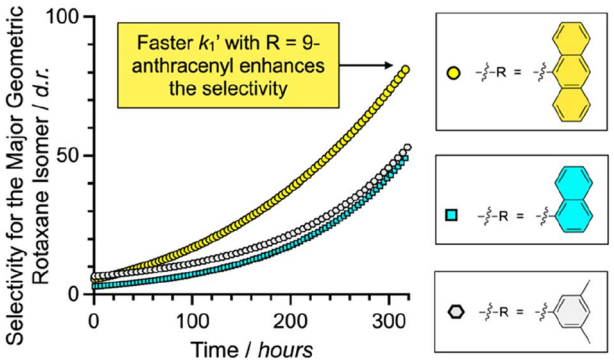

Fig. 5 Plots of the diastereoselectivity (d.r. = [RDP[5]cat@MA$_{fav}$]/[RDP[5]cat@MA$_{disfav}$]) for the major geometric rotaxane isomers formed over time for the aminolysis reactions shown in Fig. 4. The concentrations of the products were obtained from the kinetic fits to the quantitative ^{1}H NMR data shown in Fig. 3, S3b, and S5b.†

At the same time, the rate constants k_1' increased significantly from R = 3,5-dimethylbenzyl, to R = 1-naphtyl, and R = 9-anthracenyl, which is contrary to the trend observed for k_1. We hypothesize that this inverted trend is the result of reduced supramolecular interactions between the pillararene ring and the amide stoppers in the monofunctionalized rotaxane products **RDP[5]cat@MA$_{disfav}$-2** (the naphthyl case) and **RDP[5]cat@MA$_{disfav}$-3** (the anthracenyl case). This hypothesis was confirmed by DFT-calculated binding energies (Fig. 6) between the ring and the amide stoppers.

Based on the DFT results, we find that 3,5-dimethylbenzylamide stopper in **RDP[5]cat@MA$_{disfav}$-1** binds the strongest with the pillararene ring, while the 9-anthracenemethanamide and the 1-naphthalenemethanamide stoppers showed a reduced affinity with the ring.

Once again, this trend is caused by the increasing steric bulk of the initial amine nucleophiles, which ultimately leads to bulkier amide stoppers in the anthracenyl/naphthyl cases for the monofunctionalized rotaxane products **RDP[5]cat@MA$_{disfav}$**. As shown by our DFT calculations (Fig. 6), the increased steric bulk of the 9-anthracenemethanamide and the 1-naphthalenemethanamide stoppers even forces one of the methoxyl groups out of conjugation with the aromatic units on the pillararene rings. As a result, the supramolecular interaction strength between the rings and the amide stoppers is significantly reduced in the anthracenyl/naphthyl cases, which favors the co-conformations with the glyme activating groups residing over the remaining active esters. Consequently, the k_1' rate constants with **RDP[5]cat@MA$_{disfav}$-2** and **RDP[5]cat@MA$_{disfav}$-3** are faster than with **RDP[5]cat@MA$_{disfav}$-1.**

Since the fastest k_1' results with 9-anthracenemethanamine as the nucleophile, the minor geometric rotaxane isomer (**RDP[5]cat@MA$_{disfav}$**) reacts away even faster in the anthracenyl case,

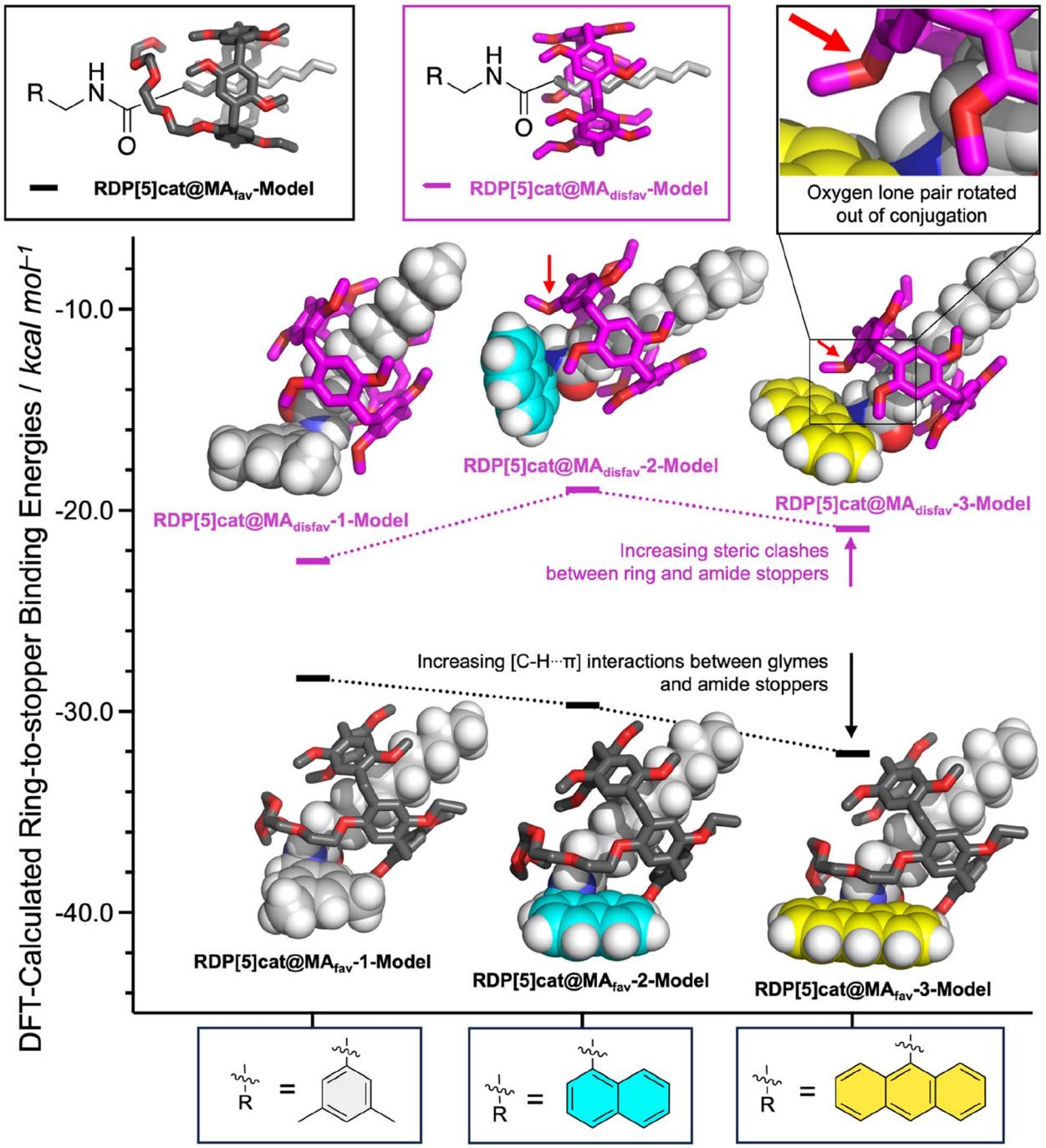

Fig. 6 DFT-calculated binding energies (B3LYP-MM/aug-cc-pVDZ//B3LYP-MM/LACVP* level of theory) between the different faces of the **RDP[5]cat** ring and the varying amide stoppers for both geometric isomers. The model systems used to calculate the binding energies are shown in insets at the top left of the figure. In the model systems for the disfavored rotaxane products (**RDP[5]cat@MA$_{disfav}$-1-Model**, **RDP[5]cat@MA$_{disfav}$-2-Model**, and **RDP[5]cat@MA$_{disfav}$-3-Model**), the tetraglyme chains do not directly interact with the varying amide stoppers. Therefore, for the models of the disfavored rotaxane products, the tetraglyme chains on the ring were replaced with ethyl substituents to simplify the conformational space and enable a more accurate search of the conformational space at the DFT level with these smaller model systems.

which further increases the selectivity for the formation of the major geometric isomer (as shown in Fig. 5) with 9-anthracenemethanamine as the nucleophile. Overall, near exponential growth of the reaction selectivity over time is observed (Fig. 5) with all three amine nucleophiles, since—as more of the desired major product forms over time—the undesired product also keeps reacting away faster than the desired product, which leads to a continuously increasing selectivity of the reaction for the major geometric isomer.

(ii) Steric effects of the ring on the aminolysis rates: While the face of the ring with the tetraglyme chains clearly speeds up the aminolysis reactions as discussed above, the

aminolysis reactions slow down when the secondary face of the ring (*i.e.*, the face without the glyme functions) is sitting over an active ester. Based on our computational model shown in Fig. 2b, we explain this slow-down effect by the simple steric bulk of the macrocycle, which partially blocks attack of the nucleophile when the secondary face of the ring is positioned over the active ester. Related inhibition effects of reactivity by the mechanical bond have been observed previously in the literature.[26]

This inhibition effect is also clearly visible when comparing the k_2 and k_2' rate constants (Fig. 3c) for the aminolysis reaction with 3,5-dimethylbenzylamine. In this case, k_2' is significantly slower than k_2, since in the monoamide **RDP[5]cat@MA$_{fav}$-1** the ring spends a significant portion of time over the active ester (based on the NOESY NMR shown in Fig. 2a), thereby partially blocking access of the nucleophile to the active ester in this monoamide. In contrast, the ring is expected to be much more evenly distributed between the two active ester sites in the starting material **RDP[5]cat@diester**, which ultimately leads to k_2 being significantly faster than k_2' with the 3,5-dimethylbenzylamine nucleophile.

At the same time, the k_2' rate constants also increased notably (Fig. 4) in the anthracenyl and naphthyl cases, compared to the case with R = 3,5-dimethylbenzyl. Again, we hypothesize that this effect is caused by the secondary face of the ring inhibiting nucleophilic attack, and by changing the balance of supramolecular interactions between the ring and the varying amide stoppers. In this case, the DFT calculations show that the tetraglyme groups interact[27] more strongly with the amide stoppers when R = naphthyl/anthracenyl than with R = 3,5-dimethylbenzyl. Therefore, the stronger supramolecular interactions between the tetraglyme groups and the aromatic stoppers in the anthracenyl/naphthyl case favor the co-conformation with the ring residing over the side of the amide stopper in the case of **RDP[5]cat@MA$_{fav}$-2** and **RDP[5]cat@MA$_{fav}$-3**, which frees up the active ester on the other end of the rotaxane for faster nucleophilic attack and leads to overall faster k_2' rate constants.

Conclusions

We developed a kinetically controlled strategy to selectively access specific geometric isomers of complex interlocked molecules through a coupled reaction system involving selective stopper exchange reactions. Our reaction system was able to achieve high selectivity by enhancing the intrinsic selectivity of the selective stopper exchange reactions based on coupled reactions of inverse selectivity. While the use of a glyme catalyst/activating group as a means of promoting stopper exchange in rotaxanes was previously reported by our group,[10] this work expands the synthetic toolbox available to selectively access rotaxane geometric isomers. We are currently applying our synthetic strategy for the synthesis of new living polymerization catalysts and are also expanding our methodology to other macrocycles and catalysts/activating groups to access complex interlocked molecules in a more effective manner.

Data availability

The datasets generated during this study are available from the authors upon reasonable request.

Author contributions

S. T. S. guided the project, performed the DFT calculations together with D. R. M. and K. X., discussed the experimental results, and wrote the paper together with D. R. M. and K. X. D. R. M., K. X., N. B., H. L., and S. B. performed the synthesis and analysed the data. All the authors discussed the results and revised the paper.

Conflicts of interest

There are no conflicts to declare.

Acknowledgements

We thank M. Ivancic for NMR support and B. O'Rourke for high-resolution mass spectrometry. Synthetic material for this research was supported by the NSF (CAREER Award CHE-1848444/2317652 awarded to STS), while the kinetic analysis was supported by the U.S. Army Research Office (Grant 71015-CH-YIP awarded to STS). Part of the computational resources were supported by the NVIDIA GPU Grant Seed Program (awarded to STS) and by the NIH (MIRA award 1R35GM147579-01). Partial support was also provided by NSF's CTMC Program *via* an NSF CAREER Award (CHE-1945394/2410514) awarded to JL. H. L. was supported by a summer undergraduate research fellowship from Middlebury College.

Notes and references

1 (*a*) V. Blanco, A. Carlone, K. D. Hänni, D. A. Leigh and B. Lewandowski, A Rotaxane-Based Switchable Organocatalyst, *Angew. Chem., Int. Ed.*, 2012, **51**, 5166–5169; (*b*) V. Blanco, D. A. Leigh, V. Marcos, J. A. Morales-Serna and A. L. Nussbaumer, A Switchable [2]Rotaxane Asymmetric Organocatalyst That Utilizes an Acyclic Chiral Secondary Amine, *J. Am. Chem. Soc.*, 2014, **136**, 4905–4908; (*c*) Y. Cakmak, S. Erbas-Cakmak and D. A. Leigh, Asymmetric Catalysis with a Mechanically Point-Chiral Rotaxane, *J. Am. Chem. Soc.*, 2016, **138**, 1749–1751; (*d*) K. Eichstaedt, J. Jaramillo-Garcia, D. A. Leigh, V. Marcos, S. Pisano and T. A. Singleton, Switching between Anion-Binding Catalysis and Aminocatalysis with a Rotaxane Dual-Function Catalyst, *J. Am. Chem. Soc.*, 2017, **139**, 9376–9381; (*e*) A. W. Heard and S. M. Goldup, Synthesis of a Mechanically Planar Chiral Rotaxane Ligand for Enantioselective Catalysis, *Chem*, 2020, **6**, 994–1006; (*f*) C. Kwamen and J. Niemeyer, Functional Rotaxanes in Catalysis, *Chem.–Eur. J.*, 2021, **27**, 175–186; (*g*) J. Y. C. Lim, N. Yuntawattana, P. D. Beer and C. K. Williams, Isoselective Lactide Ring Opening Polymerisation using [2]Rotaxane Catalysts, *Angew. Chem., Int. Ed.*, 2019, **58**, 6007–

6011; (*h*) A. Martinez-Cuezva, A. Saura-Sanmartin, M. Alajarin and J. Berna, Mechanically Interlocked Catalysts for Asymmetric Synthesis, *ACS Catal.*, 2020, **10**, 7719–7733; (*i*) A. Martinez-Cuezva, A. Saura-Sanmartin, T. Nicolas-Garcia, C. Navarro, R.-A. Orenes, M. Alajarin and J. Berna, Photoswitchable interlocked thiodiglycolamide as a cocatalyst of a chalcogeno-Baylis–Hillman reaction, *Chem. Sci.*, 2017, **8**, 3775–3780.

2 (*a*) S. Borsley, D. A. Leigh and B. M. W. Roberts, A Doubly Kinetically-Gated Information Ratchet Autonomously Driven by Carbodiimide Hydration, *J. Am. Chem. Soc.*, 2021, **143**, 4414–4420; (*b*) S. F. M. v. Dongen, S. Cantekin, J. A. A. W. Elemans, A. E. Rowan and R. J. M. Nolte, Functional interlocked systems, *Chem. Soc. Rev.*, 2013, **43**, 99–122; (*c*) S. Erbas-Cakmak, D. A. Leigh, C. T. McTernan and A. L. Nussbaumer, Artificial Molecular Machines, *Chem. Rev.*, 2015, **115**, 10081–10206; (*d*) J. Groppi, L. Casimiro, M. Canton, S. Corra, M. Jafari-Nasab, G. Tabacchi, L. Cavallo, M. Baroncini, S. Silvi, E. Fois and A. Credi, Precision Molecular Threading/Dethreading, *Angew. Chem., Int. Ed.*, 2020, **132**, 14935–14944; (*e*) E. R. Kay and D. A. Leigh, Rise of the Molecular Machines, *Angew. Chem., Int. Ed.*, 2015, **54**, 10080–10088; (*f*) J. E. M. Lewis, M. Galli and S. M. Goldup, Properties and emerging applications of mechanically interlocked ligands, *Chem. Commun.*, 2016, **53**, 298–312; (*g*) S. Mena-Hernando and E. M. Pérez, Mechanically interlocked materials. Rotaxanes and catenanes beyond the small molecule, *Chem. Soc. Rev.*, 2019, **48**, 5016–5032; (*h*) E. A. Neal and S. M. Goldup, Chemical consequences of mechanical bonding in catenanes and rotaxanes: isomerism, modification, catalysis and molecular machines for synthesis, *Chem. Commun.*, 2014, **50**, 5128–5142; (*i*) D. Sluysmans, P. Lussis, C.-A. Fustin, A. Bertocco, D. A. Leigh and A.-S. Duwez, Real-Time Fluctuations in Single-Molecule Rotaxane Experiments Reveal an Intermediate Weak Binding State during Shuttling, *J. Am. Chem. Soc.*, 2021, **143**, 2348–2352; (*j*) C. A. Stanier, S. J. Alderman, T. D. W. Claridge and H. L. Anderson, Unidirectional Photoinduced Shuttling in a Rotaxane with a Symmetric Stilbene Dumbbell, *Angew. Chem., Int. Ed.*, 2002, **41**, 1769–1772; (*k*) T. Takata, Switchable Polymer Materials Controlled by Rotaxane Macromolecular Switches, *ACS Cent. Sci.*, 2020, **6**, 129–143; (*l*) P. Wu, B. Dharmadhikari, P. Patra and X. Xiong, Rotaxane nanomachines in future molecular electronics, *Nanoscale Adv.*, 2022, **4**, 3418–3461; (*m*) B. Yao, H. Sun, L. Yang, S. Wang and X. Liu, Recent Progress in Light-Driven Molecular Shuttles, *Front. Chem.*, 2022, **9**, 832735; (*n*) H.-Y. Zhou, Q.-S. Zong, Y. Han and C.-F. Chen, Recent advances in higher order rotaxane architectures, *Chem. Commun.*, 2020, **56**, 9916–9936.

3 (*a*) M. Baroncini, S. Silvi and A. Credi, Photo- and Redox-Driven Artificial Molecular Motors, *Chem. Rev.*, 2020, **120**, 200–268; (*b*) Y. Feng, M. Ovalle, J. S. W. Seale, C. K. Lee, D. J. Kim, R. D. Astumian and J. F. Stoddart, Molecular Pumps and Motors, *J. Am. Chem. Soc.*, 2021, **143**, 5569–5591.

4 (*a*) R. J. Bordoli and S. M. Goldup, An Efficient Approach to Mechanically Planar Chiral Rotaxanes, *J. Am. Chem. Soc.*, 2014, **136**, 4817–4820; (*b*) C. Casati, P. Franchi, R. Pievo, E. Mezzina and M. Lucarini, Unraveling Unidirectional Threading of α-Cyclodextrin in a [2]Rotaxane through Spin Labeling Approach, *J. Am. Chem. Soc.*, 2012, **134**, 19108–19117; (*c*) F. d'Orchymont and J. P. Holland, Supramolecular Rotaxane-Based Multi-Modal Probes for Cancer Biomarker Imaging, *Angew. Chem., Int. Ed.*, 2022, **61**, e202204072; (*d*) E. M. G. Jamieson, F. Modicom and S. M. Goldup, Chirality in rotaxanes and catenanes, *Chem. Soc. Rev.*, 2018, **47**, 5266–5311; (*e*) M. A. Jinks, A. de Juan, M. Denis, C. J. Fletcher, M. Galli, E. M. G. Jamieson, F. Modicom, Z. Zhang and S. M. Goldup, Stereoselective Synthesis of Mechanically Planar Chiral Rotaxanes, *Angew. Chem., Int. Ed.*, 2018, **57**, 14806–14810; (*f*) Y. Makita, N. Kihara and T. Takata, Synthesis and kinetic resolution of directional isomers of [2]rotaxanes bearing a lariat crown ether wheel, *Supramol. Chem.*, 2021, **33**, 1–7; (*g*) J. R. J. Maynard and S. M. Goldup, Strategies for the Synthesis of Enantiopure Mechanically Chiral Molecules, *Chem*, 2020, **6**, 1914–1932; (*h*) K. Nakazono and T. Takata, Mechanical Chirality of Rotaxanes: Synthesis and Function, *Symmetry*, 2020, **12**, 144; (*i*) N. Pairault and J. Niemeyer, Chiral Mechanically Interlocked Molecules – Applications of Rotaxanes, Catenanes and Molecular Knots in Stereoselective Chemosensing and Catalysis, *Synlett*, 2018, **29**, 689–698.

5 (*a*) M. Bazzoni, L. Andreoni, S. Silvi, A. Credi, G. Cera, A. Secchi and A. Arduini, Selective access to constitutionally identical, orientationally isomeric calix[6]arene-based [3]rotaxanes by an active template approach, *Chem. Sci.*, 2021, **12**, 6419–6428; (*b*) P. La Manna, C. Talotta, C. Gaeta, A. Soriente, M. De Rosa and P. Neri, Threading of an Inherently Directional Calixarene Wheel with Oriented Ammonium Axles, *J. Org. Chem.*, 2017, **82**, 8973–8983.

6 (*a*) G. De Bo, M. A. Y. Gall, M. O. Kitching, S. Kuschel, D. A. Leigh, D. J. Tetlow and J. W. Ward, Sequence-Specific β-Peptide Synthesis by a Rotaxane-Based Molecular Machine, *J. Am. Chem. Soc.*, 2017, **139**, 10875–10879; (*b*) J. Echavarren, M. A. Y. Gall, A. Haertsch, D. A. Leigh, J. T. J. Spence, D. J. Tetlow and C. Tian, Sequence-Selective Decapeptide Synthesis by the Parallel Operation of Two Artificial Molecular Machines, *J. Am. Chem. Soc.*, 2021, **143**, 5158–5165.

7 J. Berná, D. A. Leigh, M. Lubomska, S. M. Mendoza, E. M. Pérez, P. Rudolf, G. Teobaldi and F. Zerbetto, Macroscopic transport by synthetic molecular machines, *Nat. Mater.*, 2005, **4**, 704–710.

8 (*a*) T. Oshikiri, Y. Takashima, H. Yamaguchi and A. Harada, Kinetic Control of Threading of Cyclodextrins onto Axle Molecules, *J. Am. Chem. Soc.*, 2005, **127**, 12186–12187; (*b*) M. Quiroga, M. Parajó, P. Rodríguez-Dafonte and L. García-Río, Kinetic Study of [2]Pseudorotaxane Formation with an Asymmetrical Thread, *Langmuir*, 2016, **32**, 6367–6375; (*c*) Q.-C. Wang, X. Ma, D.-H. Qu and H. Tian, Unidirectional

Threading Synthesis of Isomer-Free [2]Rotaxanes, *Chem.–Eur. J.*, 2006, **12**, 1088–1096; (*d*) M. Xue, Y. Yang, X. Chi, X. Yan and F. Huang, Development of Pseudorotaxanes and Rotaxanes: From Synthesis to Stimuli-Responsive Motions to Applications, *Chem. Rev.*, 2015, **115**, 7398–7501; (*e*) T. Oshikiri, Y. Takashima, H. Yamaguchi and A. Harada, Face-Selective [2]- and [3]Rotaxanes: Kinetic Control of the Threading Direction of Cyclodextrins, *Chem.–Eur. J.*, 2007, **13**, 7091–7098; (*f*) P. Waelès, M. Gauthier and F. Coutrot, Study of [2]- and [3]Rotaxanes Obtained by Post-Synthetic Aminolysis of a Kinetically Stable Carbonate-Containing Pseudorotaxane, *Eur. J. Org. Chem.*, 2022, **2022**, e202101385; (*g*) H.-X. Wang, Z. Meng, J.-F. Xiang, Y.-X. Xia, Y. Sun, S.-Z. Hu, H. Chen, J. Yao and C.-F. Chen, Guest-dependent directional complexation based on triptycene derived oxacalixarene: formation of oriented rotaxanes, *Chem. Sci.*, 2016, **7**, 469–474.

9 (*a*) M. D. Struble, M. G. Holl, G. Coombs, M. A. Siegler and T. Lectka, Synthesis of a Tight Intramolecular OH···Olefin Interaction, Probed by IR, 1H NMR, and Quantum Chemistry, *J. Org. Chem.*, 2015, **80**, 4803–4807; (*b*) M. G. Holl, M. D. Struble, P. Singal, M. A. Siegler and T. Lectka, Positioning a Carbon-Fluorine Bond over the π Cloud of an Aromatic Ring: A Different Type of Arene Activation, *Angew. Chem., Int. Ed.*, 2016, **55**, 8266–8269; (*c*) D. D. Bume, C. R. Pitts, F. Ghorbani, S. A. Harry, J. N. Capilato, M. A. Siegler and T. Lectka, Ketones as directing groups in photocatalytic sp3 C-H fluorination, *Chem. Sci.*, 2017, **8**, 6918–6923; (*d*) L. Guan, M. G. Holl, C. R. Pitts, M. D. Struble, M. A. Siegler and T. Lectka, Through-Space Activation Can Override Substituent Effects in Electrophilic Aromatic Substitution, *J. Am. Chem. Soc.*, 2017, **139**, 14913–14916; (*e*) K. E. Murphy, J. L. Bocanegra, X. Liu, H. K. Chau, P. C. Lee, J. Li and S. T. Schneebeli, Precise through-space control of an abiotic electrophilic aromatic substitution reaction, *Nat. Commun.*, 2017, **8**, 14840; (*f*) C. R. Pitts, M. G. Holl and T. Lectka, Spectroscopic Characterization of a [C-F-C]+ Fluoronium Ion in Solution, *Angew. Chem., Int. Ed.*, 2018, **57**, 1924–1927; (*g*) J. P. Campbell, S. C. Rajappan, T. J. Jaynes, M. Sharafi, Y. T. Ma, J. Li and S. T. Schneebeli, Enantioselective Electrophilic Aromatic Nitration: A Chiral Auxiliary Approach, *Angew. Chem., Int. Ed.*, 2019, **58**, 1035–1040; (*h*) M. Kazim, H. Foy, M. A. Siegler, T. Dudding and T. Lectka, Discovery and Mechanistic Study of a Totally Organic C(aryl)-C(alkyl)Oxygen Insertion Reaction, *J. Org. Chem.*, 2019, **84**, 14349–14353; (*i*) M. Kazim, M. A. Siegler and T. Lectka, A Case of Serendipity: Synthesis, Characterization, and Unique Chemistry of a Stable, Ring-Unsubstituted Aliphatic p-Quinone Methide, *Org. Lett.*, 2019, **21**, 2326–2329; (*j*) M. G. Holl, C. R. Pitts and T. Lectka, Quest for a Symmetric [C-F-C]+ Fluoronium Ion in Solution: A Winding Path to Ultimate Success, *Acc. Chem. Res.*, 2020, **53**, 265–275; (*k*) M. Kazim, L. Guan, A. Chopra, R. Sun, M. A. Siegler and T. Lectka, Switching a HO···π Interaction to a Nonconventional OH···π Hydrogen Bond: A Completed Crystallographic Puzzle, *J. Org. Chem.*, 2020, **85**, 9801–9807; (*l*) S. T. Schneebeli, M. Sharafi, J. P. Campbell, K. E. Murphy and R. Osadchey Brown, Chiral Auxiliaries for Stereoselective Electrophilic Aromatic Substitutions, *Synlett*, 2020, **32**, 229–234; (*m*) K. F. Hoffmann, A. Wiesner, C. Mueller, S. Steinhauer, H. Beckers, M. Kazim, C. R. Pitts, T. Lectka and S. Riedel, Structural proof of a [C-F-C]+ fluoronium cation, *Nat. Commun.*, 2021, **12**, 5275; (*n*) S. A. Harry, M. R. Xiang, E. Holt, A. Zhu, F. Ghorbani, D. Patel and T. Lectka, Hydroxy-directed fluorination of remote unactivated C(sp3)-H bonds: a new age of diastereoselective radical fluorination, *Chem. Sci.*, 2022, **13**, 7007–7013; (*o*) M. Kazim, Z. Feng, S. Vemulapalli, M. A. Siegler, A. Chopra, P. Minh Nguyen, M. Gargiulo Holl, L. Guan, T. Dudding, D. J. Tantillo and T. Lectka, Through-Space, Lone-Pair Promoted Aromatic Substitution: A Relay Mechanism Can Beat Out Direct Activation, *Chem.–Eur. J.*, 2023, e202301550, DOI: **10.1002/chem.202301550**; (*p*) M. Kazim, M. Wang, S. Vemulapalli, P. M. Nguyen, Y. Wang, M. A. Siegler, T. Dudding and T. Lectka, How Do Face-to-Face Stacked Aromatic Rings Activate Each Other to Electrophilic Aromatic Substitution?, *Org. Lett.*, 2023, **25**, 4318–4322; (*q*) H. J. Davis and R. J. Phipps, Harnessing non-covalent interactions to exert control over regioselectivity and site-selectivity in catalytic reactions, *Chem. Sci.*, 2017, **8**, 864–877; (*r*) W. A. Golding, R. Pearce-Higgins and R. J. Phipps, Site-Selective Cross-Coupling of Remote Chlorides Enabled by Electrostatically Directed Palladium Catalysis, *J. Am. Chem. Soc.*, 2018, **140**, 13570–13574; (*s*) W. A. Golding and R. J. Phipps, Electrostatically-directed Pd-catalysis in combination with C-H activation: site-selective coupling of remote chlorides with fluoroarenes and fluoroheteroarenes, *Chem. Sci.*, 2020, **11**, 3022–3027; (*t*) Y.-H. Li, Y. Ouyang, N. Chekshin and J.-Q. Yu, PdII-Catalyzed γ-C(sp3)-H (Hetero)arylation of Ketones Enabled by Transient Directing Groups, *ACS Catal.*, 2022, **12**, 10581–10586; (*u*) Y.-Q. Chen, S. Singh, Y. Wu, Z. Wang, W. Hao, P. Verma, J. X. Qiao, R. B. Sunoj and J.-Q. Yu, Pd-Catalyzed γ-C(sp3)-H Fluorination of Free Amines, *J. Am. Chem. Soc.*, 2020, **142**, 9966–9974; (*v*) K. Hong, H. Park and J.-Q. Yu, Methylene C(sp3)-H Arylation of Aliphatic Ketones Using a Transient Directing Group, *ACS Catal.*, 2017, **7**, 6938–6941; (*w*) Y. Wu, Y.-Q. Chen, T. Liu, M. D. Eastgate and J.-Q. Yu, Pd-Catalyzed γ-C(sp3)-H Arylation of Free Amines Using a Transient Directing Group, *J. Am. Chem. Soc.*, 2016, **138**, 14554–14557; (*x*) G. Xia, J. Weng, L. Liu, P. Verma, Z. Li and J.-Q. Yu, Reversing conventional site-selectivity in C(sp3)-H bond activation, *Nat. Chem.*, 2019, **11**, 571–577; (*y*) L.-J. Xiao, K. Hong, F. Luo, L. Hu, W. R. Ewing, K.-S. Yeung and J.-Q. Yu, PdII-Catalyzed Enantioselective C(sp3)-H Arylation of Cyclobutyl Ketones Using a Chiral Transient Directing Group, *Angew. Chem., Int. Ed.*, 2020, **59**, 9594–9600; (*z*) F.-L. Zhang, K. Hong, T.-J. Li, H. Park and J.-Q. Yu, Functionalization of C(sp3)-H bonds using a transient directing group, *Science*, 2016, **351**, 252–256; (*aa*) R.-Y. Zhu, L.-Y. Liu and J.-Q. Yu, Highly Versatile β-

C(sp3)-H Iodination of Ketones Using a Practical Auxiliary, *J. Am. Chem. Soc.*, 2017, **139**, 12394–12397.

10 S. C. Rajappan, D. R. McCarthy, J. P. Campbell, J. B. Ferrell, M. Sharafi, O. Ambrozaite, J. Li and S. T. Schneebeli, Selective Monofunctionalization Enabled by Reaction-History-Dependent Communication in Catalytic Rotaxanes, *Angew. Chem., Int. Ed.*, 2020, **59**, 16668–16674.

11 (*a*) A. Martinez-Cuezva, D. Bautista, M. Alajarin and J. Berna, Enantioselective Formation of 2-Azetidinones by Ring-Assisted Cyclization of Interlocked N-(alpha-Methyl)benzyl Fumaramides, *Angew. Chem., Int. Ed.*, 2018, **57**, 6563–6567; (*b*) M. Calles, J. Puigcerver, D. A. Alonso, M. Alajarin, A. Martinez-Cuezva and J. Berna, Enhancing the selectivity of prolinamide organocatalysts using the mechanical bond in [2]rotaxanes, *Chem. Sci.*, 2020, **11**, 3629–3635; (*c*) N. Pairault, H. Zhu, D. Jansen, A. Huber, C. G. Daniliuc, S. Grimme and J. Niemeyer, Heterobifunctional Rotaxanes for Asymmetric Catalysis, *Angew. Chem., Int. Ed.*, 2020, **59**, 5102–5107; (*d*) C. Lopez-Leonardo, A. Saura-Sanmartin, M. Marin-Luna, M. Alajarin, A. Martinez-Cuezva and J. Berna, Ring-to-Thread Chirality Transfer in [2]Rotaxanes for the Synthesis of Enantioenriched Lactams, *Angew. Chem., Int. Ed.*, 2022, **61**, e202209904.

12 S. Amano, S. D. P. Fielden and D. A. Leigh, A catalysis-driven artificial molecular pump, *Nature*, 2021, **594**, 529–534.

13 E. Liu, S. Cherraben, L. Boulo, C. Troufflard, B. Hasenknopf, G. Vives and M. Sollogoub, A molecular information ratchet using a cone-shaped macrocycle, *Chem*, 2023, **9**, 1147–1163.

14 (*a*) N. Basilio, L. García-Río, J. R. Leis, J. C. Mejuto and M. Pérez-Lorenzo, Novel catalytic effects in ester aminolysis in chlorobenzene, *Chem. Commun.*, 2005, 3817–3819, DOI: 10.1039/B504629G; (*b*) N. Basilio, L. García-Río, J. C. Mejuto and M. Pérez-Lorenzo, A New Reaction Pathway in the Ester Aminolysis Catalyzed by Glymes and Crown Ethers, *J. Org. Chem.*, 2006, **71**, 4280–4285; (*c*) R. D. Gandour, D. A. Walker, A. Nayak and G. R. Newkome, Catalysis of ester aminolysis by macrocyclic ionophores, *J. Am. Chem. Soc.*, 1978, **100**, 3608–3609; (*d*) J. C. Hogan and R. D. Gandour, The remarkable catalytic power of glymes in ester aminolysis carried out in nonpolar media, *J. Am. Chem. Soc.*, 1980, **102**, 2865–2866; (*e*) W. P. Jencks and J. Carriuolo, General Base Catalysis of the Aminolysis of Phenyl Acetate1, *J. Am. Chem. Soc.*, 1960, **82**, 675–681.

15 (*a*) R. Hertzberg, G. Monreal Santiago and C. Moberg, Synthesis of the β3-Adrenergic Receptor Agonist Solabegron and Analogous N-(2-Ethylamino)-β-amino Alcohols from O-Acylated Cyanohydrins - Expanding the Scope of Minor Enantiomer Recycling, *J. Org. Chem.*, 2015, **80**, 2937–2941; (*b*) C. Moberg, Minor enantiomer recycling - a strategy to improve enantioselectivity, *Pure Appl. Chem.*, 2016, **88**, 309–316; (*c*) Y.-Q. Wen, R. Hertzberg, I. Gonzalez and C. Moberg, Minor Enantiomer Recycling: Application to Enantioselective Syntheses of Beta Blockers, *Chem.–Eur. J.*, 2014, **20**, 3806–3812; (*d*) E. Wingstrand, A. Laurell, L. Fransson, K. Hult and C. Moberg, Minor Enantiomer Recycling: Metal Catalyst, Organocatalyst and Biocatalyst Working in Concert, *Chem.–Eur. J.*, 2009, **15**, 12107; (*e*) C. Moberg, Recycling in Asymmetric Catalysis, *Acc. Chem. Res.*, 2016, **49**, 2736–2745.

16 N. Y. Shin, J. M. Ryss, X. Zhang, S. J. Miller and R. R. Knowles, Light-driven deracemization enabled by excited-state electron transfer, *Science*, 2019, **366**, 364–369.

17 P. Demay-Drouhard, K. Du, K. Samanta, X. Wan, W. Yang, R. Srinivasan, A. C. H. Sue and H. Zuilhof, Functionalization at Will of Rim-Differentiated Pillar[5]arenes, *Org. Lett.*, 2019, **21**, 3976–3980.

18 T. Ogoshi, Synthesis of novel pillar-shaped cavitands "Pillar[5]arenes" and their application for supramolecular materials, *J. Inclusion Phenom. Macrocyclic Chem.*, 2012, **72**, 247–262.

19 (*a*) P. J. Cragg and K. Sharma, Pillar[5]arenes: fascinating cyclophanes with a bright future, *Chem. Soc. Rev.*, 2012, **41**, 597–607; (*b*) K. Yang, S. Chao, F. Zhang, Y. Pei and Z. Pei, Recent advances in the development of rotaxanes and pseudorotaxanes based on pillar[n]arenes: from construction to application, *Chem. Commun.*, 2019, **55**, 13198–13210.

20 T. Ogoshi, K. Demachi, K. Kitajima and T.-a. Yamagishi, Monofunctionalized pillar[5]arenes: synthesis and supramolecular structure, *Chem. Commun.*, 2011, **47**, 7164–7166.

21 (*a*) S. D. P. Fielden, D. A. Leigh, C. T. McTernan, B. Pérez-Saavedra and I. J. Vitorica-Yrezabal, Spontaneous Assembly of Rotaxanes from a Primary Amine, Crown Ether and Electrophile, *J. Am. Chem. Soc.*, 2018, **140**, 6049–6052; (*b*) M. Sharafi, K. T. McKay, M. Ivancic, D. R. McCarthy, N. Dudkina, K. E. Murphy, S. C. Rajappan, J. P. Campbell, Y. Shen, A. R. Badireddy, J. Li and S. T. Schneebeli, Size-Selective Catalytic Polymer Acylation with a Molecular Tetrahedron, *Chem*, 2020, **6**, 1469–1494.

22 I. Nierengarten, E. Meichsner, M. Holler, P. Pieper, R. Deschenaux, B. Delavaux-Nicot and J.-F. Nierengarten, Preparation of Pillar[5]arene-Based [2]Rotaxanes by a Stopper-Exchange Strategy, *Chem.–Eur. J.*, 2018, **24**, 169–177.

23 *Jaguar, version 8.8*, 2015.

24 E. R. Johnson, S. Keinan, P. Mori-Sanchez, J. Contreras-Garcia, A. J. Cohen and W. Yang, Revealing noncovalent interactions, *J. Am. Chem. Soc.*, 2010, **132**, 6498–6506.

25 P. Kuzmič, Program DYNAFIT for the Analysis of Enzyme Kinetic Data: Application to HIV Proteinase, *Anal. Biochem.*, 1996, **237**, 260–273.

26 (*a*) A. M. Albrecht-Gary, Z. Saad, C. O. Dietrich-Buchecker and J. P. Sauvage, Interlocked macrocyclic ligands: a kinetic catenand effect in copper(I) complexes, *J. Am. Chem. Soc.*, 1985, **107**, 3205; (*b*) A. H. Parham, B. Windisch and F. Vögtle, Chemical Reactions in the Axle of Rotaxanes – Steric Hindrance by the Wheel, *Eur. J. Org. Chem.*, 1999, **1999**, 1233–1238; (*c*) T. Oku, Y. Furusho and T. Takata, Rotaxane-stabilized thiophosphonium salt from disulfide and phosphine, *Org. Lett.*, 2003, **5**, 4923–4925; (*d*) E. A. Neal and S. M. Goldup, Chemical consequences of mechanical bonding in catenanes and rotaxanes: isomerism, modification, catalysis and molecular

machines for synthesis, *Chem. Commun.*, 2014, **50**, 5128–5142; (*e*) F. C. Hsueh, C. Y. Tsai, C. C. Lai, Y. H. Liu, S. M. Peng and S. H. Chiu, N-Heterocyclic Carbene Copper(I) Rotaxanes Mediate Sequential Click Ligations with All Reagents Premixed, *Angew. Chem., Int. Ed.*, 2020, **59**, 11278–11282; (*f*) B. Leforestier, M. R. Gyton and A. B. Chaplin, Oxidative Addition of a Mechanically Entrapped C(sp)-C(sp) Bond to a Rhodium(I) Pincer Complex, *Angew. Chem., Int. Ed.*, 2020, **59**, 23500–23504.

27 S. Zhang, W. Li, J. Luan, A. Srivastava, V. Carnevale, M. L. Klein, J. Sun, D. Wang, S. P. Teora, S. J. Rijpkema, J. D. Meeldijk and D. A. Wilson, Adaptive insertion of a hydrophobic anchor into a poly(ethylene glycol) host for programmable surface functionalization, *Nat. Chem.*, 2023, **15**, 240–247.